J|A|C|S
ARTICLES

Published on Web 04/13/2009

Spin Crossover-Coupled Electron Transfer of $[M(tacn)_2]^{3+/2+}$ Complexes (tacn = 1,4,7-Triazacyclononane; M = Cr, Mn, Fe, Co, Ni)

Richard L. Lord,[†] Franklin A. Schultz,*[,†,‡] and Mu-Hyun Baik*[,†]

Department of Chemistry, Indiana University, 800 East Kirkwood Avenue, Bloomington, Indiana 47405, and Department of Chemistry and Chemical Biology, Indiana University Purdue University Indianapolis, 402 North Blackford Street, Indianapolis, Indiana 46402

Received December 9, 2008; E-mail: fschultz@iupui.edu (F.A.S.); mbaik@indiana.edu (M.-H.B.)

Abstract: The role of spin state equilibria on the thermodynamics of electron transfer in $[M(tacn)_2]^{3+/2+}$ complexes (tacn = 1,4,7-triazacyclononane; M = Cr, Mn, Fe, Co, Ni) was examined using density functional theory at the B3LYP*/cc-pVTZ(-f) level coupled to a continuum solvation model to afford excellent agreement between computed and experimental redox properties. An intuitive explanation of the previously observed nonperiodic trend in reduction potentials, which display a sawtooth pattern along the first-row transition metal series, is offered utilizing a novel diagrammatic illustration of the relationship between spin state energetics and reduction potentials. This representation leads to a generalized proposal for analyzing and designing nearly isoenergetic spin states of transition metals in a given ligand environment. A new ligand specific parameter α that allows for quantifying the differential reduction potential as a function of the metal identity is introduced, and a novel protocol is presented that divides the ligand−metal interactions into primary and secondary characteristics, which we anticipate will be useful for rationally designing the electronics of transition metal complexes in general.

Introduction

Transition metal compounds are tremendously versatile in part due to the remarkable variance in electronic and geometric structure they can exhibit as a function of the chemical environment. The ease with which they expose different electronic structure patterns is particularly beneficial in catalysis. One such mechanism by which they dramatically modulate both the relative ordering and shapes of their frontier orbitals, which are directly responsible for chemical reactivity, is alteration of electron spin configurations. First-row transition metal complexes are well-known to be very flexible in adopting different spin states. Cases where multiple spin states are thermally accessible that may even give rise to different spin states existing in equilibrium are of great interest for applications in catalysis. Thus, the rational design of spin crossover and/or spin equilibria into catalytic cycles would be a great boon. Chemical and physical properties of complexes in different spin states are often dramatically different, even when the molecular composition is identical. Qualitatively, the relative stability of different spin states can be understood using ligand field theory, with the spectrochemical series conveniently providing a scale for the energetic splitting between the nonbonding and antibonding frontier orbitals (Δ_o). The balance between Δ_o and the electron pairing energy ultimately determines whether a low- or high-spin complex is energetically favored. Features favoring one spin state over the other, such as the compactness of the structure or metal valency, have helped rationalize observed spin states *a posteriori* with great success. An *a priori*, systematic design principle given a ligand framework has, however, heretofore been lacking. For instance, given a homoleptic system such as $[M(NH_3)_6]^{n+}$, it is impossible to determine whether a given metal, oxidation state, and chemical environment combination can enforce isoenergetic spin states without substantial experimental trial and error. Here we propose an efficient strategy for discovering and fine-tuning such systems. Whereas we consider this work to be merely a first step toward designing spin state equilibria in a truly rational fashion, we expect the proposed analysis and design protocols to be generally valid and universally applicable.

We have recently shown that some of the simplest coordination compounds, homoleptic Cr^{II} cyano complexes $[Cr^{II}(CN)_x]^{2-x}$ ($x = 5$ or 6), can be challenging to understand as the intrinsic M−L binding electronics and Coulombic forces between metal and ligands combine in a nontrivial fashion.[1] The most critical factor for rationalizing the unexpected accessibility of the high-spin state in these compounds is the difficulty of bringing six negatively charged ligands into close proximity about Cr^{II}. The extent to which these Coulombic forces dominate the overall free energy of the species, in relation to the ligand field splitting due to the metal−ligand interactions, is intimately linked to the identity and oxidation state of both the metal and ligand. Thus, an ideal platform for investigating strategies and protocols for a rational design of spin state energetics as a function of the metal and ligand charges are spin crossover-coupled redox systems, where the preference for either low- or high-spin configurations can be disturbed by injecting or removing an electron electrochemically.[2] In addition to these conceptual

[†] Indiana University.
[‡] Indiana University Purdue University Indianapolis.

(1) Lord, R. L.; Baik, M.-H. *Inorg. Chem.* **2008**, *47*, 4413–4420.

considerations, spin crossover-coupled electron transfer is an interesting and poorly understood phenomenon that plays an important role in both chemical and biological systems, where it often controls the spontaneity and selectivity of critical reactions.[3−10] One of us has shown experimentally that incorporation of spin state changes can markedly influence the thermodynamics and kinetics of heterogeneous electron transfer reactions.[3,11−13]

In this work, we examined the redox properties and spin state energetics of a series of $[M(tacn)_2]^{3+/2+}$ complexes (tacn = 1,4,7-triazacyclononane; M = Cr, Mn, Fe, Co, Ni). While density functional theory (DFT) coupled to a continuum solvation model has been demonstrated to be reliable for predicting reduction potentials of transition metal complexes without complicating chemical equilibria coupled to the redox event,[14] the treatment of spin states by DFT is more problematic.[15−32] Thus, it is important that the electrochemical and magnetic properties of these complexes are relatively well established,[11,33−37] allowing our computational results to be meaningfully compared with experiments. An empirical observation for the *bis*-tacn complexes, and many other first-row transition metal compounds, is the "sawtooth" behavior in reduction potential going from Mn to Co,[12] reminiscent of the abrupt jump in gas-phase electron attachment energies when approaching the half-filled electron shell.[38−40] We demonstrate the origin of this nonperiodic behavior from first principles and put forth a novel analysis scheme that allows for systematic understanding of spin crossover-coupled redox thermodynamics.

Computational Details

All calculations were carried out using DFT as implemented in the Jaguar 7.0 suite of quantum chemistry programs.[41] Geometry optimizations were performed at the B3LYP*/6-31G** level of theory[16,42−45] with transition metals represented using the Los Alamos LACVP basis.[46−48] Energies computed with the double-ζ basis set are not reliable for redox phenomena, as was previously reported.[14] Subsequent single-point energies were conducted with Dunning's correlation consistent triple-ζ basis set, cc-pVTZ(-f),[49] with transition metals represented using LACV3P, a decontracted version of LACVP to match the effective core potential with a triple-ζ quality basis. In addition to the B3LYP* functional, BLYP and B3LYP were also used to evaluate the spin state energies. B3LYP* was found to deliver results that were most consistent with experimental results. Comparisons to BLYP and B3LYP, representing extremes of low- and high-spin stabilization, respectively, have been relegated to the Supporting Information (Appendix S1). Multireference calculations at the complete active space self-consistent field (CASSCF) level have also been performed using Molpro[50] version 2006.1 using the 6-31G**/LACVP basis set (Appendix S2) for the four Fe complexes $^{HS}Fe^{II}$, $^{LS}Fe^{II}$, $^{HS}Fe^{III}$, and $^{LS}Fe^{III}$. Solvation energies were computed at the double-ζ level using a self-consistent reaction field approach based on numerical solutions of the Poisson−Boltzmann equation.[51−53] These were computed at the optimized gas-phase geometries utilizing an appropriate dielectric constant for comparison to experimental conditions (ε = 80.37 for water). The standard set of optimized radii in Jaguar was employed: Cr (1.511 Å), Mn (1.480 Å), Fe (1.456 Å), Co (1.436 Å), Ni (1.417 Å), H (1.150 Å), C (1.900 Å), N (1.600 Å).[54] Analytical vibrational frequencies within the

(2) Gütlich, P.; Goodwin, H. A. *Spin crossover in transition metal compounds*; Springer: Berlin, 2004; Vols. *I*−*III*.
(3) Turner, J. W.; Schultz, F. A. *Coord. Chem. Rev.* **2001**, *219*−*221*, 81–97.
(4) Yoder, J. C.; Roth, J. P.; Gussenhoven, E. M.; Larsen, A. S.; Mayer, J. M. *J. Am. Chem. Soc.* **2003**, *125*, 2629–2640.
(5) Meunier, B.; de Visser, S. P.; Shaik, S. *Chem. Rev.* **2004**, *104*, 3947–3980.
(6) Shaik, S.; Kumar, D.; de Visser, S. P.; Altun, A.; Thiel, W. *Chem. Rev.* **2005**, *105*, 2279–2328.
(7) Battistuzzi, G.; Bellei, M.; Zederbauer, M.; Furtmueller, P. G.; Sola, M.; Obinger, C. *Biochemistry* **2006**, *45*, 12750–12755.
(8) Noodleman, L.; Han, W.-G. *J. Biol. Inorg. Chem.* **2006**, *11*, 674–694.
(9) Mader, E. A.; Davidson, E. R.; Mayer, J. M. *J. Am. Chem. Soc.* **2007**, *129*, 5153–5166.
(10) Das, A.; Grinkova, Y. V.; Sligar, S. G. *J. Am. Chem. Soc.* **2007**, *129*, 13778–13779.
(11) Turner, J. W.; Schultz, F. A. *J. Phys. Chem. B* **2002**, *106*, 2009–2017.
(12) De Alwis, D. C. L.; Schultz, F. A. *Inorg. Chem.* **2003**, *42*, 3616–3622.
(13) Hossain, F.; Rigsby, M. A.; Duncan, C. T.; Milligan, P. L.; Lord, R. L.; Baik, M.-H.; Schultz, F. A. *Inorg. Chem.* **2007**, *46*, 2596–2603.
(14) Baik, M.-H.; Friesner, R. A. *J. Phys. Chem. A* **2002**, *106*, 7407–7415.
(15) Paulsen, H.; Trautwein, A. X. *Top. Curr. Chem.* **2004**, *235*, 197–220.
(16) Reiher, M.; Salomon, O.; Hess, B. A. *Theor. Chem. Acc.* **2001**, *107*, 48–55.
(17) Salomon, O.; Reiher, M.; Hess, B. A. *J. Chem. Phys.* **2002**, *117*, 4729–4737.
(18) Reiher, M. *Inorg. Chem.* **2002**, *41*, 6928–6935.
(19) Swart, M.; Groenhof, A. R.; Ehlers, A. W.; Lammertsma, K. *J. Phys. Chem. A* **2004**, *108*, 5479–5483.
(20) Deeth, R. J.; Fey, N. *J. Comput. Chem.* **2004**, *25*, 1840–1848.
(21) Fouqueau, A.; Mer, S.; Casida, M. E.; Daku, L. M. L.; Hauser, A.; Mineva, T.; Neese, F. *J. Chem. Phys.* **2004**, *120*, 9473–9486.
(22) Fouqueau, A.; Casida, M. E.; Daku, L. M. L.; Hauser, A.; Neese, F. *J. Chem. Phys.* **2005**, *122*, 044110.
(23) Ganzenmuller, G.; Berkaine, N.; Fouqueau, A.; Casida, M. E.; Reiher, M. *J. Chem. Phys.* **2005**, *122*, 234321.
(24) Daku, L. M. L.; Vargas, A.; Hauser, A.; Fouqueau, A.; Casida, M. E. *ChemPhysChem* **2005**, *6*, 1393–1410.
(25) Paulsen, H.; Wolny, J. A.; Trautwein, A. X. *Monatsh. Chem.* **2005**, *136*, 1107–1118.
(26) Pierloot, K.; Vancoillie, S. *J. Chem. Phys.* **2006**, *125*, 124303.
(27) Rong, C. Y.; Lian, S. X.; Yin, D. L.; Shen, B.; Zhong, A. G.; Bartolotti, L.; Liu, S. B. *J. Chem. Phys.* **2006**, *125*, 174102.
(28) Zein, S.; Borshch, S. A.; Fleurat-Lessard, P.; Casida, M. E.; Chermette, H. *J. Chem. Phys.* **2007**, *126*, 014105.
(29) Conradie, J.; Ghosh, A. *J. Chem. Theory Comput.* **2007**, *3*, 689–702.
(30) Wasbotten, I. H.; Ghosh, A. *Inorg. Chem.* **2007**, *46*, 7890–7898.
(31) Pierloot, K.; Vancoillie, S. *J. Chem. Phys.* **2008**, *128*, 034104.
(32) Güell, M.; Luis, J. M.; Solà, M.; Swart, M. *J. Phys. Chem. A* **2008**, *112*, 6384–6391.
(33) Wieghardt, K.; Schmidt, W.; Herrmann, W.; Kueppers, H. J. *Inorg. Chem.* **1983**, *22*, 2953–2956.
(34) Crawford, P. W.; Schultz, F. A. *Inorg. Chem.* **1994**, *33*, 4344–4350.
(35) Turner, J. W.; Schultz, F. A. *Inorg. Chem.* **1999**, *38*, 358–364.
(36) Turner, J. W.; Schultz, F. A. *Inorg. Chem.* **2001**, *40*, 5296–5298.
(37) Chaudhuri, P.; Wieghardt, K. *Prog. Inorg. Chem.* **1987**, *35*, 329–436.
(38) Griffith, J. S. *The theory of transition-metal ions.* University Press: Cambridge, U.K., 1964.
(39) van Gaal, H. L. M.; van der Linden, J. G. M. *Coord. Chem. Rev.* **1982**, *47*, 41–54.
(40) Richardson, D. E.; Ryan, M. F.; Khan, M. N. I.; Maxwell, K. A. *J. Am. Chem. Soc.* **1992**, *114*, 10482–10485.
(41) *Jaguar 7.0*; Schrödinger, LLC: New York, NY, 2007.
(42) Becke, A. D. *Phys. Rev. A* **1988**, *38*, 3098–3100.
(43) Lee, C. T.; Yang, W. T.; Parr, R. G. *Phys. Rev. B* **1988**, *37*, 785–789.
(44) Becke, A. D. *J. Chem. Phys.* **1993**, *98*, 5648–5652.
(45) Stephens, P. J.; Devlin, F. J.; Chabalowski, C. F.; Frisch, M. J. *J. Phys. Chem.* **1994**, *98*, 11623–11627.
(46) Hay, P. J.; Wadt, W. R. *J. Chem. Phys.* **1985**, *82*, 270–283.
(47) Wadt, W. R.; Hay, P. J. *J. Chem. Phys.* **1985**, *82*, 284–298.
(48) Hay, P. J.; Wadt, W. R. *J. Chem. Phys.* **1985**, *82*, 299–310.
(49) Dunning, T. H., Jr. *J. Chem. Phys.* **1989**, *90*, 1007–1023.
(50) Werner, H. J.; Knowles, P. J.; Lindh, R.; Schuetz, M., et al. (see http://www.molpro.net). *MOLPRO*, version 2006.1, a package of ab initio programs.
(51) Friesner, R. A.; Murphy, R. B.; Beachy, M. D.; Ringnalda, M. N.; Pollard, W. T.; Dunietz, B. D.; Cao, Y. X. *J. Phys. Chem. A* **1999**, *103*, 1913–1928.
(52) Marten, B.; Kim, K.; Cortis, C.; Friesner, R. A.; Murphy, R. B.; Ringnalda, M. N.; Sitkoff, D.; Honig, B. *J. Phys. Chem.* **1996**, *100*, 11775–11788.
(53) Edinger, S. R.; Cortis, C.; Shenkin, P. S.; Friesner, R. A. *J. Phys. Chem. B* **1997**, *101*, 1190–1197.

harmonic approximation were computed with the double-ζ basis for thermodynamics analysis and to ensure all stationary points were well-defined minima.

Thermodynamic properties were obtained as summarized in eqs 1−4, with standard approximations assumed for the entropy corrections in the gas phase.[55] The defined enthalpy, ΔH(gas), neglects the thermal corrections that we previously found to be negligible. The entropy of the solvent enters implicitly through $\Delta\Delta G_{solv}$, and ΔS(gas) only contains contributions from the solute. Solution phase free energies are obtained by adding the free energy of solvation to the gas phase free energy. Zero-point energies and entropy corrections were derived using unscaled harmonic frequencies. All potentials have been referenced against NHE (alternatively called SHE)[56] using a value of 4.43 V[57] to stay consistent with earlier work in our laboratory.[14] The absolute potential of NHE is still a debated topic, with values ranging from 4.28 to 4.43 V (using both experimental and theoretical estimates).[57−61] Bearing this in mind, there may be systematic errors in our computed potentials up to 150 mV.

$$\Delta H(\text{gas}) = \Delta E(\text{SCF}) + \Delta\text{ZPE} \quad (1)$$

$$\Delta G(\text{gas}) = \Delta H(\text{gas}) - 298.15\ \text{K} * \Delta S(\text{gas}) \quad (2)$$

$$\Delta G(\text{sol}) = \Delta G(\text{gas}) + \Delta\Delta G_{solv} \quad (3)$$

$$\Delta G^{EA}(\text{sol}) = -n\text{FE}^\circ \quad (4)$$

ΔH(gas) = gas phase enthalpy; ΔE(SCF) = electronic energy; ΔZPE = zero-point energy correction; ΔG(gas) = gas phase Gibbs free energy; ΔS(gas) = gas phase entropy; ΔG(sol) = solution phase free energy; $\Delta\Delta G_{solv}$ = free energy of solvation; ΔG^{EA}(sol) = solvated free energy of reduction; E° = standard reduction potential; n = number of electrons; F = Faraday constant.

Results and Discussion

Bis-tacn complexes of the first-row transition metals Cr, Mn, Fe, Co, and Ni have a variety of electron configuration choices. Because the metal lies within a pseudo-octahedral ligand field, metal d orbitals herein are discussed within this approximation; i.e., the frontier orbitals are labeled as t_{2g} and e_g orbitals. It is important to establish which of the most plausible spin states, either low spin (LS) or high spin (HS), is adopted as a function of metal d electron count. By LS we imply $S = 1$ for d^4, $S = {}^1/_2$ for d^5, $S = 0$ for d^6, and $S = {}^1/_2$ for d^7; for HS it is $S = 2$ for d^4, $S = {}^5/_2$ for d^5, $S = 2$ for d^6, and $S = {}^3/_2$ for d^7. Two metal oxidation states have no reasonable alternative spin states: Cr^{III} adopts an $S = {}^3/_2$ configuration with the t_{2g} set of orbitals half-filled, while Ni^{II} is $S = 1$ with the e_g set of orbitals half-filled.

Despite the widespread success of DFT for various applications, the accurate prediction of spin state energy differences in transition metal complexes remains a difficult challenge.[15−32] This problem is relatively well understood, and there is general agreement that the standard formulation of the hybrid functionals, such as B3LYP, significantly overestimates the exchange energy (which is by definition only nonzero for parallel spin electrons) whereas pure functionals, such as BLYP, underestimate the contribution of exchange to the total energy. As a consequence B3LYP routinely overestimates the stability of HS systems while BLYP gives unwarranted preference to LS complexes. Unfortunately, there is currently no way of systematically improving the functionals to more appropriately treat spin state energetics. One popular *ad hoc* improvement has been to reduce the amount of Hartree−Fock (HF) exchange in hybrid functionals. Reiher and co-workers observed that reducing HF exchange in B3LYP from its original 20% to 15% significantly improves the accuracy of DFT for predicting the energies of different spin states of transition metal complexes. This modified functional is denoted B3LYP*. We tested B3LYP, B3LYP*, and BLYP and observe that B3LYP* gives results that best agree with the experimental data. Thus, most of our discussion is based on the B3LYP* results.

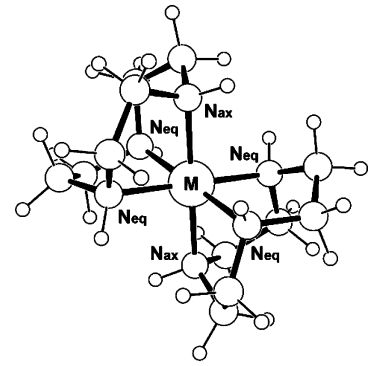

Figure 1. Typical structure of a $[M(tacn)_2]^{n+}$ complex.

Structural Features. The computed bond lengths and angles in the pseudo-octahedral coordination sphere are enumerated in Table 1 for the seven species where direct comparison to crystallographic data is possible. Table S1 (Supporting Information) contains these metrics for all of the computed species, and Cartesian coordinates are tabulated in Table S2. All species exhibit M−N bond lengths consistent with electron occupation. Notably, the HS d^4 complexes (Cr^{II} and Mn^{III}) and LS d^7 complexes (Co^{II} and Ni^{III}), each with asymmetric occupation of the e_g orbital set, display large Jahn−Teller distortions. B3LYP* overestimated bond lengths by 0.05−0.10 Å consistent with previous findings.[18] Three metrics for the bond angles were tracked: $N-M-N_{intra}$ for the intraligand angles, and $N-M-N_{trans}$ and $N-M-N_{inter}$ for *trans* and *cis* interligand angles, respectively. The largest deviation from experimentally determined angles was ∼10° ($N-{}^{HS}Mn^{II}-N_{inter}$), though all others are off by only 3−4°, within the reasonable agreement between theory and experiment. While a direct comparison to experimental values for the *bis*-tacn complexes of $^{HS}Mn^{III}$, Cr^{III}, or $^{HS}Cr^{II}$ was not possible, the M−N contact distances of 2.187,[62] 2.133, and 2.500/2.205 Å are consistent with values of 2.125, 2.075, and 2.670/2.118 Å measured for the related compounds $[Mn^{III}(sarcophagine)](NO_3)_3$,[63,64] $[Cr^{III}(N,N',N''$-

(54) Rashin, A. A.; Honig, B. *J. Phys. Chem.* **1985**, *89*, 5588–5593.
(55) Cramer, C. J. *Essentials of computational chemistry: theories and models*, 2nd ed.; J. Wiley: Hoboken, NJ, 2004.
(56) Bard, A. J.; Faulkner, L. R. *Electrochemical Methods*; John Wiley & Sons, Inc.: New York, 1980.
(57) Reiss, H.; Heller, A. *J. Phys. Chem.* **1985**, *89*, 4207–4213.
(58) Tissandier, M. D.; Cowen, K. A.; Feng, W. Y.; Gundlach, E.; Cohen, M. H.; Earhart, A. D.; Coe, J. V.; Tuttle, T. R. *J. Phys. Chem. A* **1998**, *102*, 7787–7794.
(59) Tissandier, M. D.; Cowen, K. A.; Feng, W. Y.; Gundlach, E.; Cohen, M. H.; Earhart, A. D.; Tuttle, T. R.; Coe, J. V. *J. Phys. Chem. A* **1998**, *102*, 9308–9308.
(60) Zhan, C.-G.; Dixon, D. A. *J. Phys. Chem. A* **2001**, *105*, 11534–11540.
(61) Kelly, C. P.; Cramer, C. J.; Truhlar, D. G. *J. Phys. Chem. B* **2006**, *110*, 16066–16081.
(62) Computed axial and equitorial bond lengths were averaged to compare the trigonal prismatic experimental structure to the JT distorted octahedral computed structure.
(63) Creaser, I. I.; Engelhardt, L. M.; Harrowfield, J. M.; Sargeson, A. M.; Skelton, B. W.; White, A. H. *Aust. J. Chem.* **1993**, *46*, 465–476.
(64) Anderson, P. A.; Creaser, I. I; Dean, C.; Harrowfield, J. M.; Horn, E.; Martin, L. L.; Sargeson, A. M.; Snow, M. R.; Tiekink, E. R. T. *Aust. J. Chem.* **1993**, *46*, 449–463.

Table 1. Select Optimized Structural Parameters for $[M(tacn)_2]^{n+}$ with Crystallographic Values in Parentheses[a]

	$^{HS}Mn^{II}$	$^{LS}Fe^{II}$	$^{LS}Fe^{III}$	$^{HS}Co^{II}$	$^{LS}Co^{III}$	Ni^{II}	$^{LS}Ni^{III}$
N−M	2.321	2.084	2.049	2.226	2.019	2.179	2.219/2.027
	(2.278)	(2.034)	(1.998)	(2.160)	(1.968)	(2.106)	(2.109/1.971)
$N-M-N_{intra}$	77.0	82.6	83.4	79.6	84.0	80.5	82.1/84.0
	(77.6)	(83.8)	(84.2)	(82.2)	(85.5)	(82.6)	(83.7/85.8)
$N-M-N_{trans}$	179.4	179.6	179.7	179.1	179.6	179.5	178.9/179.5
	(180.0)	(179.4)	(179.2)	(178.3)	(178.8)	(178.1)	(178.0/177.3)
$N-M-N_{inter}$	103.0	97.4	96.6	100.4	96.0	99.5	98.0/96.1
	(93.7)	(95.9)	(96.2)	(97.8)	(94.5)	(97.5)	(96.4/94.3)
CSD[b] code	CEXNUP[67]	DETTOL[68]	DETTUR01[69]	DOTZUH[70]	WUDVEW[71]	BAZNNI[72]	DORTIN[70,73]

[a] For low-spin Ni^{III}, axial and equatorial values are listed separately: $M-N_{ax}/M-N_{eq}$ for bond lengths, $N_{ax}-M-N_{eq}/N_{eq}-M-N_{eq}$ for *cis* angles, $N_{ax}-M-N_{ax}/N_{eq}-M-N_{eq}$ for *trans* angles. Bond lengths in Å, angles in degrees. [b] CSD = Cambridge Structural Database.

tris(aminoethyl)-1,4,7-triazacyclononane)]$(NO_3)(ClO_4)$,[65] and $[Cr^{II}(o\text{-phenylenediamine})_3]Br_2$,[66] respectively.

Overall, bond lengths decrease across the first-row, with increasing oxidation state, and with a change from high- to low-spin configuration. Most significant in terms of its structural impact is spin crossover. Partial occupation of strongly antibonding e_g orbital(s) in the HS states results in considerable M−N elongation, to ∼2.2 Å or longer, with the shortest contacts displayed by late metals like Ni (2.179 and 2.171 Å for Ni^{II} and $^{HS}Ni^{III}$, respectively) and the longest contacts adopted by early period metals like $^{HS}Cr^{II}$ and $^{HS}Mn^{II}$ (2.303 and 2.321 Å, average of ax/eq values). Concurrent with this bond elongation is a further deviation of 3°−4° from perfect angular arrangement (90°) due to constraints of the heterocyclic ligand; as the M−N distance increases, the facial capping ligand is unable to properly occupy three sites of the perfect octahedron without energetically costly rearrangement of the tacn backbone. Oxidized complexes tend to be more disposed toward a perfect octahedral ligand environment than M^{II}, as measured by $N-M-N_{intra}$ and $N-M-N_{inter}$. On average, this change in bond angle with oxidation state is 1°−2° when decoupled from spin crossover. Importantly, in addition to shorter M−N contacts due to electrostatic attraction, angular arrangement of the ligand field implies a larger expected preference for LS configurations in the oxidized compounds. This salient feature of the tethered amines in tacn was explored in relation to free ammines (*vide infra*). $N-M-N_{trans}$ is nearly linear for all species (±1° computed, ±3° crystal).

Spin Crossover Thermodynamics. To properly describe electron transfer thermodynamics, we must ensure that spin state thermodynamics are accurately reproduced. A common concern is that open shell systems may become multiconfigurational, which is impossible to model correctly with the approximate functionals currently available within the single determinant formulation of DFT. In these cases, multireference methods like CASSCF are more appropriate, but they are computationally much more expensive and technically more challenging. We have examined the $Fe^{II/III}$ complexes using CASSCF and found that the leading and only significant CI coefficient (>0.5) was 0.976, 1.000, 0.954, and 0.999 for $^{LS}Fe^{II}$, $^{HS}Fe^{II}$, $^{LS}Fe^{III}$, and $^{HS}Fe^{III}$ at their respective DFT optimized geometries. Denoting the orbitals as $\varphi(1)\varphi(2)$ for M−L e_g σ, $\varphi(3)\varphi(4)\varphi(5) = t_{2g}$ nonbonding, and $\varphi(6)\varphi(7)$ = M−L e_g σ^*, the configuration state functions ($|\varphi(1)\varphi(2)\varphi(3)\varphi(4)\varphi(5)\varphi(6)\varphi(7)>$) were $|2222200>$, $|222aaaa>$, $|2222a00>$, and $|22aaaaa>$, respectively, confirming that the electronic structure of the $[Fe(tacn)_2]^{n+}$ compounds, at their respective minima, are single reference and use of the single reference DFT methodology is justified. DFT energy differences (HS − LS, $\Delta G(sol)_{SC}$) using BLYP, B3LYP*, and B3LYP and the corresponding spin equilibrium constants (K_{SC}) based on the B3LYP* results are listed in Table 2. As anticipated, BLYP overestimates the stability of the LS states substantially, whereas B3LYP gives inconsistently low HS state energies. B3LYP* results are also as anticipated between these two extremes and give remarkably plausible results, qualitatively reproducing all trends of the spin state thermodynamics that have been characterized. Therefore, we use the B3LYP* results for all of our discussion below.

Table 2. Spin Crossover Equilibrium Thermodynamics for All Species with Variable Spin State (d^4 to d^7)

	$\Delta G(sol)_{SC}$ (kcal mol^{-1})			K_{SC}
	BLYP	**B3LYP***	B3LYP	**B3LYP***
Cr^{II} - d^4	−11.79	**−12.91**	−14.79	$\mathbf{2.9 \times 10^{9}}$
Mn^{III} - d^4	2.47	**−1.90**	−4.04	$\mathbf{3.2 \times 10^{1}}$
Mn^{II} - d^5	−25.05	**−36.01**	−40.66	$\mathbf{3.2 \times 10^{28}}$
Fe^{III} - d^5	21.10	**10.43**	6.01	$\mathbf{2.3 \times 10^{-8}}$
Fe^{II} - d^6	9.15	**0.64**	−5.23	$\mathbf{3.4 \times 10^{-1}}$
Co^{III} - d^6	52.36	**43.70**	38.88	$\mathbf{9.3 \times 10^{-33}}$
Co^{II} - d^7	4.94	**−1.62**	−5.04	$\mathbf{1.5 \times 10^{1}}$
Ni^{III} - d^7	30.04	**30.37**	28.79	$\mathbf{5.5 \times 10^{-23}}$

Our calculations suggest that the high spin configuration is favored for Cr^{II}, Mn^{III}, Mn^{II}, and Co^{II}, while low spin is computed to be the lowest energy configuration for Fe^{II}, Fe^{III}, Co^{III}, and Ni^{III}. Experimentally these predictions have been established for all but Cr^{II}, Mn^{III}, and Mn^{II},[33,36] though the structural comparisons in the previous section strongly implicate a $^{HS}Mn^{II}$ ion. Quantitatively, only the spin equilibrium constant for $[Fe(tacn)_2]^{2+}$ has been measured ($K_{SC} = 0.25$)[36] which agrees remarkably well with the value predicted by DFT ($K_{SC} = 0.34$). Whereas DFT is not expected to give such quantitative agreement, and the match in absolute number must be considered fortuitous, it is clearly reproducing the fact that this equilibrium constant is nearly 1, implying that inclusion of the spin crossover thermodynamics is vital to a proper description of the redox couple $[Fe(tacn)_2]^{3+/2+}$.[3]

(65) Endicott, J. F.; Perkovic, M. W.; Heeg, M. J.; Ryu, C. K.; Thompson, D. *Adv. Chem. Ser.* **1997**, *253*, 199–220.
(66) Jubb, J.; Larkworthy, L. F.; Oliver, L. F.; Povey, D. C.; Smith, G. W. *J. Chem. Soc., Dalton Trans.* **1991**, 2045–2050.
(67) Kromm, A.; Sheldrick, W. S. *Acta Crystallogr., Sect. E* **2007**, *63*, m581–m583.
(68) Boeyens, J. C. A.; Forbes, A.; Hancock, R. D.; Wieghardt, K. *Inorg. Chem.* **1985**, *24*, 2926–2931.
(69) Marsh, R. *Acta Crystallogr., Sect. B* **1987**, *43*, 174–178.
(70) Kueppers, H. J.; Neves, A.; Pomp, C.; Ventur, D.; Wieghardt, K.; Nuber, B.; Weiss, J. *Inorg. Chem.* **1986**, *25*, 2400–2408.
(71) Wang, Q.; Yan, S.; Liao, D.; Jiang, Z.; Cheng, P.; Leng, X.; Wang, H. *J. Mol. Struct.* **2002**, *608*, 49–53.
(72) Zompa, L. J.; Margulis, T. N. *Inorg. Chim. Acta* **1978**, *28*, L157–L159.
(73) Wieghardt, K.; Walz, W.; Nuber, B.; Weiss, J.; Ozarowski, A.; Stratemeier, H.; Reinen, D. *Inorg. Chem.* **1986**, *25*, 1650–1654.

The prediction of the correct spin state energies is encouraging, but for the purpose of this study it is more meaningful to partition the computed systems into three classes: those with (*i*) multiple accessible spin states ($K_{SC} < 10^{\pm 2}$), (*ii*) reasonably accessible spin alternatives ($10^{\pm 2} < K_{SC} < 10^{\pm 20}$), and (*iii*) completely inaccessible spin isomers ($K_{SC} > 10^{\pm 20}$). Among the complexes with readily accessible spin configurations, Fe^{II} has the most well-established and documented spin flexibility.[74] While not as extensive, Mn^{III} has also been shown to exhibit spin crossover in similar systems.[75] Recently, $^{LS}Mn^{III}$ in a MN_6 environment was observed for several polypyrazolylborate ligands.[13] Thus the weaker field strength of tacn affording an equilibrium slightly in favor of the HS configuration is reasonable. Co^{II} spin crossover complexes are also known,[76,77] but more pertinent are previous spectroscopic and computational studies demonstrating that the LS state lies low in energy.[78−81] Less accessible, but still attainable, are the low- and high-spin states of Cr^{II} and Fe^{III}, respectively. Fe^{III} has been observed to afford complexes exhibiting spin crossover.[82] Typically these examples involve coordination environments possessing relatively weak ligand field effects, such as FeN_4O_2 and FeS_6.[3,83] The HS state would need to be significantly stabilized for Fe^{II} for spin equilibrium in Fe^{III} to exist, in direct contrast to the findings here where the LS state is slightly favored in Fe^{II}. Spin state accessibility for Cr^{II} is less well documented,[75,84] being a fringe case for spin equilibrium (d^4), and *bona fide* low-spin examples typically involve relatively strong field ligands like CN^-.[85] Recently, experimental[86] and theoretical[1,87] work on homoleptic cyano Cr^{II} species in nonaqueous solution documented that the low-spin hexacyano species is kinetically well-defined, though thermodynamically unstable. Lability of the sixth cyanide ligand is facilitated by concurrent spin crossover to the high-spin $[Cr(CN)_5]^{3-}$ complex in the absence of coordinating cations. Finally, Mn^{II}, Co^{III} (aside from the extraordinarily weak O_6 ligand field afforded by Kläui-type ligands),[88−90] and Ni^{III} strictly demonstrate a single spin state. Why should these electronic configurations be dominated by a single spin state?

The d^5 $^{HS}Mn^{II}$ ion is significantly more stable than its LS spin isomer due to the half-filled $t_{2g}^3e_g^2$ electron occupation pattern. This overwhelming stability of $^{HS}Mn^{II}$ has been well-established, even in the gas phase.[38] Similarly, $^{LS}Co^{III}$ completely fills the t_{2g} manifold as a d^6 ion. When compared to the Fe^{II} species, also LS d^6 but barely so ($K_{SC} \cong 0.3$), the shorter M−N contacts (2.019 vs 2.084 Å) along with more rigorously octahedral angles $N-M-N_{intra}$ (82.6° vs 84.0°) plausibly explain the significant spin state splitting increase. Consideration of isoelectronic Co^{II} helps rationalize the spin state splitting for Ni^{III}. For Co^{II} one would predict the HS state to be significantly stabilized due the fact that (*i*) the HS state is not expected to be Jahn−Teller distorted and (*ii*) it has a half-filled e_g orbital occupation. The flexibility of tacn to undergo a slipping motion, however, effectively nullifies the first point, as the equatorial bond lengths remain relatively short (2.059 Å) despite large axial elongation (2.309 Å). Furthermore both states have antibonding orbitals occupied. Average bond lengths for the two states are 2.142 and 2.226 Å, respectively; thus the spin state splitting only favors $^{HS}Co^{II}$ by 1.6 kcal mol^{-1}. Evidence for crossover to the LS state down to 100 K was not observed by Wieghardt et al.,[33] which is surprising given the magnitude of the energetic gap between the states. The difference in entropy between the two species, however, is much smaller than that for Fe^{II}, Fe^{III}, and Co^{III}, which all involve an angular momentum change of $\Delta S = 2$ and no e_g occupation in the LS state. According to our calculations, lower temperatures will not lead to a spin crossover event in the absence of cooperative effects in the solid state (still favors $^{HS}Co^{II}$ by 0.2 kcal mol^{-1} at 0 K). Regardless, the two states should be quite close in energy, and thus the relative stabilization (destabilization) of the LS (HS) state for Ni^{III} is reasonable given the much shorter M−N contacts due to the increase in oxidation state. This is seen in the M−N bond lengths of 2.142, 2.226, 2.091, and 2.171 Å for $^{LS}Co^{II}$, $^{HS}Co^{II}$, $^{LS}Ni^{III}$, and $^{HS}Ni^{III}$, respectively. In conclusion, the computed spin state energies are plausible in all cases and can be rationalized in a straightforward fashion.

Scheme 1. Square Scheme Decoupling Spin Crossover (Horizontal) from Electron Transfer (Vertical)

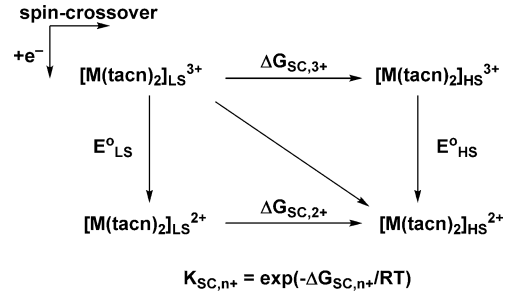

Electron Transfer Thermodynamics. Unlike the study of simple electron transfer in organometallics using DFT which demonstrated a benchmark accuracy of ∼150 mV, the electron transfer potentials investigated here must be adjusted for coupled chemical equilibria. Having firmly established the spin crossover properties of the $[M(tacn)_2]^{n+}$ systems, a meaningful discussion regarding electron transfer (occasionally coupled to spin crossover) is now possible. The general approach to the calculations is illustrated in the theoretical square scheme shown in Scheme 1, where the energies of electron transfer and spin crossover are considered separately.

Using either $E°_{LS}$ ($E°$ for $[M(tacn)_2]_{LS}^{3+} + e^- \rightarrow [M(tacn)_2]_{LS}^{2+}$) or $E°_{HS}$ ($E°$ for $[M(tacn)_2]_{HS}^{3+} + e^- \rightarrow [M(tacn)_2]_{HS}^{2+}$), the effective electrode potential (computed $E°_{comp}$ or experimental $E°_{obs}$) may be expressed, using the Nernst equation, as

(74) Gütlich, P.; Goodwin, H. A. *Top. Curr. Chem.* **2004**, *233*, 1–47.
(75) Garcia, Y.; Gütlich, P. *Top. Curr. Chem.* **2004**, *234*, 49–62.
(76) Goodwin, H. A. *Top. Curr. Chem.* **2004**, *234*, 23–47.
(77) Krivokapic, I.; Zerara, M.; Daku, M. L.; Vargas, A.; Enachescu, C.; Ambrus, C.; Tregenna-Piggott, P.; Amstutz, N.; Krausz, E.; Hauser, A. *Coord. Chem. Rev.* **2007**, *251*, 364–378.
(78) Larsson, S.; Staahl, K.; Zerner, M. C. *Inorg. Chem.* **1986**, *25*, 3033–3037.
(79) Geselowitz, D. A. *Inorg. Chim. Acta* **1989**, *163*, 79–86.
(80) Newton, M. D. *J. Phys. Chem.* **1991**, *95*, 30–38.
(81) Endres, R. G.; LaBute, M. X.; Cox, D. L. *J. Chem. Phys.* **2003**, *118*, 8706–8714.
(82) van Koningsbruggen, P. J.; Maeda, Y.; Oshio, H. *Top. Curr. Chem.* **2004**, *233*, 259–324.
(83) Nihei, M.; Shiga, T.; Maeda, Y.; Oshio, H. *Coord. Chem. Rev.* **2007**, *251*, 2606–2621.
(84) Halepoto, D. M.; Holt, D. G. L.; Larkworthy, L. F.; Povey, D. C.; Smith, G. W.; Leigh, G. J. *Polyhedron* **1989**, *8*, 1821–1822.
(85) Eaton, J. P.; Nicholls, D. *Transition Met. Chem.* **1981**, *6*, 203–206.
(86) Nelson, K. J.; Giles, I. D.; Shum, W. W.; Arif, A. M.; Miller, J. S. *Angew. Chem., Int. Ed.* **2005**, *44*, 3129–3132.
(87) Deeth, R. J. *Eur. J. Inorg. Chem.* **2006**, 2551–2555.
(88) Gütlich, P.; McGarvey, B. R.; Kläui, W. *Inorg. Chem.* **1980**, *19*, 3704–3706.
(89) Navon, G.; Kläui, W. *Inorg. Chem.* **1984**, *23*, 2722–2725.
(90) Kläui, W.; Eberspach, W.; Gütlich, P. *Inorg. Chem.* **1987**, *26*, 3977–3982.

$$E^{\circ}_{comp/obs} = E^{\circ}_{LS} + (RT/F)\ln[x_{LS,3+}/x_{LS,2+}] = E^{\circ}_{HS} + (RT/F)\ln[x_{HS,3+}/x_{HS,2+}] \quad (5)$$

where $x_{LS,n+} = (1 + K_{SC,n+})^{-1}$ and $x_{HS,n+} = K_{SC,n+}(1 + K_{SC,n+})^{-1}$ are the mole fractions of each spin state in a given oxidation state.[3] Table 3 enumerates both the spin crossover-coupled (in bold) and pure electron transfer half-reaction potentials for each species.

Computed reduction potentials (accounting for equilibria) compare favorably with experimental values. Wieghardt and coworkers measured redox potentials for the 3+/2+ couple to be −1.14 and +0.62 V vs NHE for Cr and Mn with 0.1 M $LiClO_4$ and 0.1 M KCl supporting electrolyte in water.[33] The Mn measurements must be carefully interpreted, however, as they were collected using fast scan rates and low temperature (276 K) due to chemical irreversibility.[91] Referenced against NHE, half-reaction potentials of +0.13, −0.40, and +0.95 V were measured experimentally for Fe, Co, and Ni with 0.2 M NaF supporting electrolyte in water and corrected for ion pairing.[34] Using a continuum description for water, DFT predicts reduction potentials of −0.991, +0.462, +0.136, −0.385, and +0.970 V for Cr, Mn, Fe, Co, and Ni, respectively. The largest error is ∼160 mV, similar to errors previously observed,[14] though remarkable agreement is seen for Fe, Co, and Ni.

The results in Table 3 illustrate the profound influence of the spin states on the redox chemistry. As mentioned above, reduced species typically favor HS configurations while oxidized species favor LS spin states. Because of the intimate relationship between spin decoupled electron transfer and spin crossover thermodynamics, $-nF(E^{\circ}_{HS} - E^{\circ}_{LS}) = \Delta G_{SC,2+} - \Delta G_{SC,3+}$ (see Scheme 1), the spin state energy dependence on oxidation state change has direct implications for the relative potential ordering. Thus, E°_{HS} is more positive than E°_{LS} for each metal investigated, though by differing amounts. These differences are remarkable, being as large as 2 V for Co and as small as 400 mV for Fe. Ultimately, the observed potentials reflect the avoidance of high energy species—the $^{LS}M^{II}$ state for Cr and Mn and the $^{HS}M^{III}$ state for Co and Ni. Given the spin state preferences, coupled electron transfer and spin crossover predominantly proceed from the $^{LS}M^{III}$ state to $^{HS}M^{II}$. This expectation is most clearly evidenced by the $Co^{III/II}$ couple.[92] However, the mechanism of such reactions is unclear and has been extensively debated.[93−99] The results in Tables 2 and 3 provide insight into likely intermediates in these coupled processes. Prohibitively high energy intermediates $^{LS}Mn^{II}$ and $^{HS}Co^{III}$ suggest that the reaction pathways are

$$^{LS}Mn^{III} \leftrightarrows {}^{HS}Mn^{III} \quad (6)$$

$$^{HS}Mn^{III} + e^- \rightarrow {}^{HS}Mn^{II} \quad (7)$$

and

$$^{LS}Co^{III} + e^- \rightarrow {}^{LS}Co^{II} \quad (8)$$

$$^{LS}Co^{II} \leftrightarrows {}^{HS}Co^{II} \quad (9)$$

The energetics of coupled electron transfer and spin crossover is much more fluid in the case of iron, because both intermediate spin states ($^{HS}Fe^{II}$ and $^{HS}Fe^{III}$) are more easily achieved, consistent with experimental findings.[74,82] Moreover, one of us has probed the mechanism of coupled electron transfer and spin crossover through measurement of electrochemical activation parameters. Our interpretation suggested the HS pathway to be favored in all cases;[11] however, the computed spin state energy requirements suggest reevaluation of this question.

Inspection of the potential ordering (−0.991 < −0.385 < +0.136 < +0.462 < +0.970; Cr < Co < Fe < Mn < Ni), which demonstrates the classic sawtooth behavior across the first-row metals (as illustrated in Figure 2) provides no clear trends. Attempts to rationalize the relative ease with which these complexes accept an electron based on classic electron counting principles were quickly discarded, even though the 17/18 electron vs 18/19 electron rationale for the 0.5 V difference in reduction potentials between Fe and Co is appealing. If attention is restricted to Cr, Fe, and Ni, a trend emerges; compounds are more easily reduced as we move from left to right through the first-row metals, in agreement with the expected increase in

Table 3. Half-Reaction Potentials, Referenced against NHE, for Low- and High-Spin $[M(tacn)_2]^{3+/2+}$, as well as the Equilibrium Adjusted Potential (in Bold)

half-reaction	E°_{comp} vs NHE (V)	E°_{obs} vs NHE (V)
$Cr^{III} + e^- \rightarrow {}^{LS}Cr^{II}$	−1.551	
$Cr^{III} + e^- \rightarrow {}^{HS}Cr^{II}$	−0.991	
$Cr^{III} + e^- \rightarrow Cr^{II}$	**−0.991**	**−1.14**
$^{LS}Mn^{III} + e^- \rightarrow {}^{LS}Mn^{II}$	−1.016	
$^{HS}Mn^{III} + e^- \rightarrow {}^{HS}Mn^{II}$	+0.463	
$Mn^{III} + e^- \rightarrow Mn^{II}$	**+0.462**	**+0.62**
$^{LS}Fe^{III} + e^- \rightarrow {}^{LS}Fe^{II}$	+0.129	
$^{HS}Fe^{III} + e^- \rightarrow {}^{HS}Fe^{II}$	+0.554	
$Fe^{III} + e^- \rightarrow Fe^{II}$	**+0.136**	**+0.13**
$^{LS}Co^{III} + e^- \rightarrow {}^{LS}Co^{II}$	−0.457	
$^{HS}Co^{III} + e^- \rightarrow {}^{HS}Co^{II}$	+1.508	
$Co^{III} + e^- \rightarrow Co^{II}$	**−0.385**	**−0.40**
$^{LS}Ni^{III} + e^- \rightarrow Ni^{II}$	+0.970	
$^{HS}Ni^{III} + e^- \rightarrow Ni^{II}$	+2.287	
$Ni^{III} + e^- \rightarrow Ni^{II}$	**+0.970**	**+0.95**

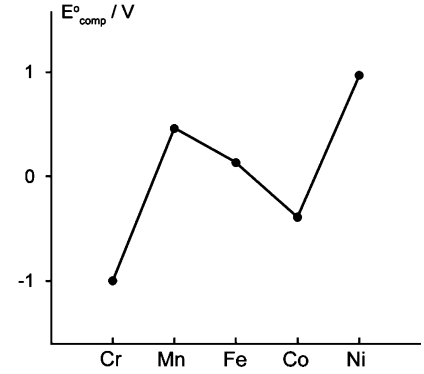

Figure 2. Computed redox potentials of $[M(tacn)_2]^{3+/2+}$ complexes in V vs NHE.

(91) $[Mn(tacn)_2]^{n+}$ calculations assume $T = 276.15$ K so direct comparison to the experimental results may be made.
(92) Hendry, P.; Ludi, A. *Adv. Inorg. Chem.* **1990**, *35*, 117–198.
(93) Buhks, E.; Bixon, M.; Jortner, J.; Navon, G. *Inorg. Chem.* **1979**, *18*, 2014–2018.
(94) Endicott, J. F.; Brubaker, G. R.; Ramasami, T.; Kumar, K.; Dwarakanath, K.; Cassel, J.; Johnson, D. *Inorg. Chem.* **1983**, *22*, 3754–3763.
(95) Hammershoi, A.; Geselowitz, D.; Taube, H. *Inorg. Chem.* **1984**, *23*, 979–982.
(96) Shalders, R. D.; Swaddle, T. W. *Inorg. Chem.* **1995**, *34*, 4815–4820.
(97) Beattie, J. K.; Elsbernd, H. *Inorg. Chim. Acta* **1995**, *240*, 641–644.
(98) Bernhardt, P. V.; Jones, L. A.; Sharpe, P. C. *Inorg. Chem.* **1997**, *36*, 2420–2425.
(99) Swaddle, T. W. *Chem. Rev.* **2005**, *105*, 2573–2608.

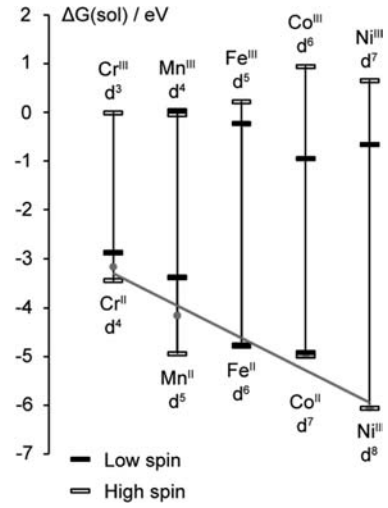

Figure 3. Relative energies of each spin/oxidation state combination for the $[M(tacn)_2]^{n+}$ compounds. The zero-points are set to be the average energy of the LS (filled) and HS (unfilled) states for the M^{III} complexes. Linear regression of the average M^{II} energies: $f(x) = -0.660x - 2.640$; $R^2 = 0.96$, where x represents the increase in atomic number.

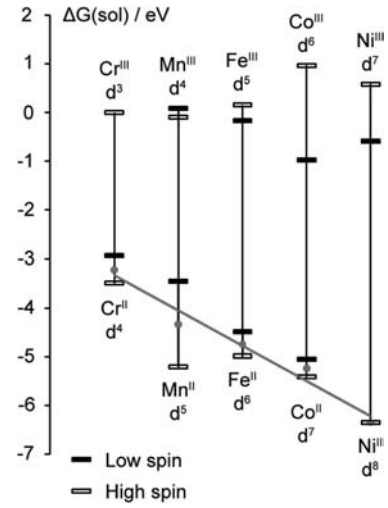

Figure 4. Relative energies of each spin/oxidation state combination for the $[M(NH_3)_6]^{n+}$ compounds. The zero points are set to be the average energy of the LS (filled) and HS (unfilled) states for the M^{III} complexes. Linear regression of the average M^{II} energies: $f(x) = -0.720x - 2.615$; $R^2 = 0.97$, where x represents the increase in atomic number.

effective nuclear charge. The simplistic correlation in Figure 2 that neglects the different spin states present, however, cannot adequately justify the potential ordering.

To properly account for the spin states within the redox framework and find a more intuitive trend, a number of possible correlations were explored (see Appendix S3). We empirically arrived at the most useful correlation, which is shown in Figure 3. Solution-phase free energies of the LS (filled) and HS (unfilled) states for each oxidation state and metal are displayed therein. The average of the LS and HS state energies of each M^{III} complex defines the energetic zero point for that metal, and the relative energies of the M^{II} complexes are shown in relation to these reference points. When plotted in this fashion, a clear trend appears that is reminiscent of the one established for electron attachment energies of the bare metal ions.[38] The average relative energies of the reduced species decrease linearly as we move from Cr to Ni. Linear regression analysis demonstrates an R^2 value of 0.96, statistically justifying this qualitative correlation. This is equivalent to taking the average of E°_{LS} and E°_{HS} and plotting this spin-averaged potential against the increasing nuclear charge. E°_{LS} involves injection of a β electron (t_{2g}) for early TMs (Cr, Mn, Fe) and an α electron (e_g*) for late TMs (Co, Ni), while E°_{HS} oppositely involves an α electron (e_g*) for early TMs (Cr, Mn) and a β electron (t_{2g}) for late TMs (Fe, Co, Ni). The average potential equates to addition of $^1/_2$ α and $^1/_2$ β for all metals but Fe, which involves addition of a β electron in both spin states. Thus, averaging E°_{LS} and E°_{LS} approximately evens out the distinct electronic environments accessed as the metal and spin state change, making the potentials comparable.

The slope of the trend line (α) seems to be physically meaningful, serving as a characteristic metric of the ligand environment. In the case of two tacn ligands α is -660 mV/metal, indicating that the chemical driving force for reduction increases by 660 mV for each group in the first-row transition metals; thus, the reduction potentials become more positive by this amount for each subsequent step to the right in the periodic table. It is important to remember, however, that this represents the *average* energy of the spin states, a quantity that by itself does not have a well-defined physical interpretation. For some of the oxidation states, namely Mn^{II}, Co^{III}, and to a lesser but notable extent Ni^{III}, deviations from the general trend are caused by large spin state splittings. These spin state splittings have a decisive impact on the relative ordering of the potentials; the reduction of Mn^{III} is significantly more favorable, and the reduction of Co^{III} significantly less favorable, due to the trend-breaking stability of $^{HS}Mn^{II}$ and $^{LS}Co^{III}$ (*vide supra*), respectively.

Thus, the correlation diagram shown in Figure 3 unifies all five metal complexes in a plausible manner and clearly identifies why Mn and Co do not follow the approximately linear trend for the reduction potential to become more positive as we move from left to right in the periodic table. This energetic scenario is surprising. Aufbau-type arguments suggest that the largest spin state splitting would arise for d^5 and d^6 systems throughout, since HS d^5 represents the special situation of having perfectly half-filled d-orbitals (both t_{2g} and e_g), while the LS d^6 case doubly occupies the t_{2g} orbitals, leaving the antibonding e_g orbitals empty. If applicable, the largest spin state splitting should be found for Mn^{II} and Fe^{III} in favor of HS and for Fe^{II} and Co^{III} in favor of the LS configuration. Ligand field arguments, on the other hand, argue for a larger preference for LS configurations as one proceeds to the right in the first-row metals due to the more intimate metal−ligand contacts. Clear exceptions to this rule are also observed; the spin state splitting in Ni^{III} is smaller than Co^{III}, and similarly Co^{II} exhibits less preference for the LS state than Fe^{II}. A systematic, yet simple, design strategy inspired by Figure 3, which simultaneously disseminates all relevant information regarding the spin and redox state, would thus be of great utility if it could also help assess the specific role of the *bis*-tacn environment.

Role of tacn for Spin State Control. Aided by the visual clarity provided by the graph shown in Figure 3, we can address more quantitatively how the tacn ligand impacts α, the slope of the average stability of M^{II}, and how it changes the spin state splittings in each of the complexes. To do so, we repeated our calculations replacing the two tridentate tacn ligands by six ammine ligands. Figure 4 shows the analogous spin state correlation diagram for the $[M(NH_3)_6]^{n+}$ systems. Interestingly, the general pattern of the diagram is fully maintained; i.e., the largest spin state splittings are observed in Mn^{II} and Co^{III}, while

Mn^{III}, Fe^{III}, Fe^{II}, and Co^{II} show relatively small energy differences between the HS and LS configurations. α has now changed to −720 mV, 60 mV more negative than before, reflecting the ∼10% differential thermodynamic driving force for reduction, with NH_3 favoring the reduced species relative to tacn. We propose that this metric is an important characteristic of a ligand system as we move forward in developing rational strategies for controlling spin in redox systems. Future work will elaborate on the utility of this parameter, beyond the intuitive demonstration presented here.

Figures 3 and 4 demonstrate an important insight into how ligands control the spin state energetics of transition metal complexes. It is useful to divide the nature of the ligands into two classes, primary and secondary characteristics. Primary characteristics consist of (*i*) the identity of the contact element (N), (*ii*) the charge of the ligand (neutral), and (*iii*) the hybridization of the contact atom (sp^3). The remaining structural and electronic features fall under the umbrella of the secondary characteristics. Primary characteristics determine the overall shape and general pattern of the relative energetics. In the examples discussed above, the six ammine and two tacn ligands share primary characteristics and the spin-averaged energy plots are consequentially approximately identical. Secondary features, such as tethering of the contact atoms into a multidentate unit or functionalization of the ligand, modulate the relative energies notably, but they are second-order effects that cannot override the overall pattern. In other words, using neutral, N-based sp^3 σ-donor ligands, it is impossible to overcome the intrinsically large spin state splitting created for Mn^{II}, Co^{III}, and Ni^{III} complexes. The realization that the basic spin state splitting pattern is determined by the primary characteristics of the ligands combined with the ability of computing spin state energetics to a sufficient degree of accuracy with the B3LYP*/cc-pVTZ(-f) model chemistry suggests a general workflow. When designing and/or analyzing transition metal complexes with different spin states, it is useful to first construct a minimal system (such as the ammine compounds) which reproduces the primary characteristics with as little decoration as possible.

There are three main differences between the tacn and ammine ligand systems: (*i*) compared to $[M(NH_3)_6]^{n+}$, the M−N bond is consistently shorter by 0.032 Å on average in $[M(tacn)_2]^{n+}$; (*ii*) because three N-atoms are tethered to afford one tacn ligand, the N−M−N angles deviate from the ideal 90°, as described above; and (*iii*) the tethering in tacn enforces an orientation of the R_2NH fragment, and thus the N donor lone pair, that is not found in the absence of structural restriction. These ligand features provide a handle for tweaking spin state energetics, in particular for metals where multiple spin states are accessible, and possibly even reversing the energetic order between them. Whereas it is nearly impossible to quantify these effects experimentally, they can be analyzed easily by a series of calculations. Starting from the fully optimized $[M(NH_3)_6]^{n+}$ geometries, we constructed two intermediary models. First, we moved the ammine nitrogens to positions that are found in the tacn complexes and optimized only the ammine hydrogens to afford the $[M(NH_3')_6]^{n+}$ models. Second, we rotated the ammine groups as to align the N−H bonds along the N−C and N−H vectors in the $[M(tacn)_2]^{n+}$ complexes to give the $[M(NH_3*)_6]^{n+}$ models.

Examining the energy evolution within this series, we can deconvolute the impact of the secondary features of the ligand on the spin state energetics. These results are summarized in Table 4 and quantify the range of energies that can be accessed by secondary ligand characteristics. In general, we find that the tacn ligand shifts the relative order in favor of the LS state throughout the series. The largest change of 10.6 kcal mol^{-1} from the $[M(NH_3)_6]^{n+}$ model is seen in $[Fe^{II}(tacn)_2]^{2+}$, where it leads to an inversion of the energy ordering. In the $[Fe^{II}(NH_3)_6]^{2+}$ model the HS state is preferred by 8.0 kcal mol^{-1}, but the LS becomes more favorable by 2.6 kcal mol^{-1} in $[Fe^{II}(tacn)_2]^{2+}$. The smallest impact is seen in the Mn^{III} system, where the overall energy change is still significant at 4.9 kcal mol^{-1}. Whereas this energy range accessible by modifying the secondary characteristics of the ligand is substantial and translates to changes of up to 6−7 orders of magnitude in the spin equilibrium constant K_{SC}, they are intrinsically smaller than the spin state energy differences determined by the primary characteristics. In other words, spin state energy differences that can be as large as ∼35 kcal mol^{-1} in Mn^{II} and Co^{III} systems disqualify these metals and oxidation states from being viable candidates for a spin crossover system in the presence of neutral, N-donor sp^3-hybridized σ-donors. The evolution of the energy differences within the model series $[M(NH_3)_6]^{n+} \rightarrow [M(NH_3')_6]^{n+} \rightarrow [M(NH_3*)_6]^{n+} \rightarrow [M(tacn)_2]^{n+}$ illustrates that all three variables, i.e., M−N distance, NHR_2 orientation, and the electronic impact of having the C_2H_4 units present in the ligand, have energetic effects of similar magnitude. A complete analysis of the origin of these effects are beyond the scope of this work, but it is clear that a decomposition of the secondary ligand characteristics in this manner will be a valuable strategic tool for precisely quantifying how the specific ligands modulate the spin state energetics.

Table 4. Electronic Spin State Energy Gaps ($\Delta E_{SC}(SCF) = E_{HS}(SCF) - E_{LS}(SCF)$) for the NH_3, NH_3', NH_3*, and tacn Complexes in kcal mol^{-1} [a]

	Mn^{III}	Mn^{II}	Fe^{III}	Fe^{II}	Co^{III}	Co^{II}
$[M(NH_3)_6]^{n+}$	−5.72	−35.79	2.95	−7.98	36.97	−8.23
Δ	2.00	2.68	6.21	5.70	4.77	−0.12
$[M(NH_3')_6]^{n+}$	−3.72	−33.11	9.16	−2.28	41.74	−8.35
Δ	2.27	1.31	4.54	2.79	3.62	5.19
$[M(NH_3*)_6]^{n+}$	−1.45	−31.80	13.70	0.51	45.36	−3.16
Δ	0.60	3.78	−2.35	2.10	−0.07	3.07
$[M(tacn)_2]^{n+}$	−0.85	−28.02	11.35	2.61	45.29	−0.09
$\Delta\Delta E_{SC}(SCF)$	4.87	7.77	8.40	10.59	8.32	8.14

[a] Δ values are with respect to the row immediately preceding, and the $\Delta\Delta E_{SC}(SCF)$ values reflect the sum of these (i.e., $NH_3 \rightarrow$ tacn).

Conclusions

This work represents significant progress toward establishing systematic approaches to understanding and designing redox active transition metal complexes that display spin state flexibility as a function of metal valency. We found that the previously proposed protocol for studying redox processes in solution phase with standard density functional theory coupled to continuum solvation models can be extended to spin crossover systems, for which the standard B3LYP functional predicts potentials in error by hundreds of millivolts. This was demonstrated by extensively benchmarking the thermodynamics of the $[M(tacn)_2]^{3+/2+}$ complexes (M = Cr to Ni). In our attempt to rationalize the nonperiodic, sawtooth behavior of the reduction potential orderings, a new diagram for correlating redox energies and spin states was arrived at empirically which allows for immediate visual comprehension of the intimate relationship and impact that spin state and reduction potential have upon one another. It was ultimately the overwhelming electronic stabilization of the HS d^5 Mn^{II} ion and the LS d^6 Co^{III} ion which

resulted in their reduction potentials being more positive and negative than otherwise expected, respectively. Linear regression of the average M^{II} energies gave a slope characteristic of the ligand environment, which we expect to be an important metric as we move forward in our development of a protocol for rationally designing spin configurations into transition metal complexes. It must be cautioned, however, that this relationship was arrived at empirically and there is no rigorous, *a priori* justification for why such a trend between the average energies of the low- and high-spin states should hold for all pseudo-octahedral complexes (though ongoing measurements are encouraging). Extension to other coordination environments will almost certainly warrant more sophisticated ways of accounting for the accessible spin states. Ultimately, the main utility of this graph is the ability to rapidly relate the spin state and redox potential for a given set of ligands, which has been accomplished.

Based on our analysis of the state averaged graphs (Figures 3 and 4), we identified two classes of ligand parameters which are critical for understanding spin state and redox thermodynamics. First, and most significant, are the primary characteristics that consist of the contact atom(s) identity, ligand charge, and contact atom(s) hybridization. These features are responsible for the gross features of the graphs, as demonstrated for ammine as compared to tacn. Of great interest for predicting spin crossover systems, the primary characteristics indicate which metal/oxidation state combinations, given a particular ligand system, have spin state splittings ($K_{SC} \leq 10$) which can be sufficiently tweaked by secondary modifications to invoke spin crossover ($K_{SC} \leq 1$). Secondary characteristics of a ligand include incorporation into a multidentate framework, to impose geometric and electronic constraints, and functionalization of the ligand to influence the electronic signature of the contact atom(s). A simple workflow allows for rapid screening of metal/ligand/oxidation state combinations with model compounds exhibiting the primary characteristics, such that a platform would then exist where subtle tuning of the secondary characteristics allows for computationally aided, rational design of the spin state and redox potentials.

Acknowledgment. We thank the NSF (CHE-0645381 and 0116050) for financial support. M.-H.B. is a Cottrell Scholar of the Research Corporation and an Alfred P. Sloan Fellow of the Alfred P. Sloan Foundation. RLL thanks the Merck Research Corporation for a graduate fellowship and Prof. Krishnan Raghavachari for helpful discussions.

Supporting Information Available: Comparison of DFT functionals, CASSCF calculations, the Cartesian coordinates, detailed energies for all species and additional discussion. This material is available free of charge via the Internet at http://pubs.acs.org.

JA809552P